Appl. Phys. B (2013) 113:417–421
DOI 10.1007/s00340-013-5479-1

Applied Physics B
Lasers and Optics

Laser-induced microjet: wavelength and pulse duration effects on bubble and jet generation for drug injection

Hun-jae Jang · Mi-ae Park · Fedir V. Sirotkin · Jack J. Yoh

Published online: 24 May 2013

Abstract The expansion of the laser-induced bubble is the main mechanism in the developed microjet injector. In this study, Nd:YAG and Er:YAG lasers are used as triggers of the bubble formation. The impact of the laser parameters on the bubble dynamics is studied and the performance of the injector is evaluated. We found that the main cause of the differences in the bubble behavior comes from the pulse duration and wavelength. For Nd:YAG laser, the pulse duration is very short relative to the bubble lifetime making the behavior of the bubble close to that of the cavitation bubble, while in Er:YAG case, the high absorption in the water and long pulse duration change the initial behavior of the bubble making it close to a vapor bubble. The contraction and subsequent rebound are typical for cavitation bubbles in both cases. The results show that the laser-induced microjet injector generates velocity which is sufficient for the drug delivery for both laser beams of different pulse duration. We estimate the typical velocity within 30–80 m/s range and the breakup length to be larger than 1 mm suitable for trans-dermal drug injection.

1 Introduction

The use of needle-free injection may potentially remedy known drawbacks such as needle phobia and possible contamination from reuse of needles [1–3]. A drug delivery system based on the microjet can penetrate topmost skin layer by using the kinetic energy of a microjet [4, 5].

H. Jang · M. Park · F. V. Sirotkin · J. J. Yoh (✉)
School of Mechanical and Aerospace Engineering, Seoul National University, Seoul 151-744, Korea
e-mail: jjyoh@snu.ac.kr

Generation of a microjet is possible in several ways. Use of an actuator based on spring, gas powered, Lorentz-force, piezoelectric element, or laser has been reported [2, 4–6]. We revisit the laser-induced microjet injector [5, 6] where a laser beam is focused inside a small container filled with water. A bubble forms upon the laser irradiation, and expansion of the bubble pushes the membrane separating drug from driving liquid, causing fast ejection of the drug. The discharged liquid forms a jet with the typical velocity in 20–100 m/s range. The dynamics of bubble depends on laser parameters such as wavelength and pulse duration [7–9]. In particular, the resulting penetration depth, which determines performance of the microjet injector, depends on the jet velocity and jet length.

In this study, Nd:YAG and Er:YAG lasers are compared for analyzing the efficiency of the microjet device. The paper is divided into two parts. First part deals with dynamics of bubble generated by the laser beams of different wavelength and pulse duration. Both dimensional and dimensionless analyses are used to understand the dependence of bubble characteristics on the laser parameters by using images taken from high-speed camera. Second part deals with the characteristics of jets and their relation to the driving bubble that allows the microjet ejection for drug delivery.

2 Experimental set up

Two experiments that are performed are (1) formation and evolution of the laser-induced bubble in a water tank and (2) generation of the microjet. The applied lasers used are skin treatment lasers (Spectra Nd:YAG and Action Er:YAG by Lutronics Co., Korea). In both experiments, we use the same laser energy of 408 mJ, while wavelength and

the pulse duration are kept different. The Nd:YAG laser has wavelength of 1064 nm and the pulse duration of 7 ns, while the Er:YAG laser has 2940 nm wavelength and pulse duration of 250 μs. Both lasers have built-in focusing system with focal length of 78 mm (Nd:YAG) and 67 mm (Er:YAG). The high-speed camera Phantom V.710 is used for visualization.

In the first experiment, the laser is focused into the water tank of 10 × 5.5 × 5.5 cm in dimension. The difference in wavelength leads to a different penetration depth $\delta_p = 1/\alpha$, where α is the absorption coefficient. For the given wavelength, the optical penetration depths are 1.65 cm and 0.8 μm for Nd:YAG and Er:YAG, respectively [10]. Because of high water absorption in Er:YAG case, the bubble forms near to the water surface. In order to isolate the bubble from ambient air, the interface is kept separate by a glass (MgF_2) window. The process of bubble development is recorded by the high-speed camera at 90,909 fps in the Nd:YAG case and at 28,986 fps in the Er:YAG case.

A schematic of the microjet injector experiment is given in Fig. 1. The laser is focused inside of the chamber which contains a driving liquid (water). The generated bubble gives rise to chamber pressure and pushes the elastic membrane which separates the drug reservoir underneath the membrane from upper driving liquid chamber. The membrane deflection pushes the drug out of the reservoir through a nozzle. The discharging liquid forms a jet. The process of microjet development is recorded by a high-speed camera at 37,016 fps in the Nd:YAG case and at 42,001 fps for the Er:YAG case, respectively.

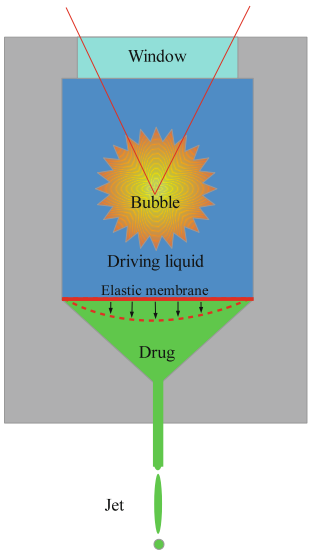

Fig. 1 Schematic of the microjet generation experiment using an injector with 150-μm nozzle

3 The bubble dynamics

The bubble dynamics is essential for the present microjet device. The expansion of the bubble starts with the formation of an initial nucleus. The nucleus is formed at a spot where the optical breakdown occurs. The energy of the laser pulse per unit area increases toward the focal point and, at some distance, the laser energy density reaches breakdown threshold. The shape of the bubble nuclei is far from spherical because it is affected by the spherical aberrations [11].

The behavior of the bubble triggered by the Er:YAG beam is distinct from that of Nd:YAG. Since the optical penetration depth is much shorter for Er:YAG laser, the beam cannot penetrate deeper into the water. Instead, the bubble starts growing from the water surface. To prevent the pressurized gas inside the bubble from interacting with the water surface, a transparent window is used to keep the vapor from escaping.

The sequential images of the bubble development in both cases are given in Fig. 2. The temporal evolution of the bubble radius is given in Fig. 3 with black dots where vertical bars illustrate the error. The behavior of the bubble which is triggered by Nd:YAG laser is typical to that observed in many studies, while Er:YAG case is seemingly distinct.

The temporal dependence of the radius in Nd:YAG case can be approximated with a well-known equation:

$$R = R_{\max}\left[\sin\left(\frac{\pi(t-t_0)}{\tau_l}\right)\right]^{1/3} \tag{1}$$

where $\tau_l = 249 \pm 18$ μs is the bubble lifetime, t_0 is the shift between the first captured image and the start of the bubble expansion. The high-speed camera and the laser are not synchronized so that $t_0 \leq 27.02$ μs and $t_0 \leq 23.81$ μs in Nd:YAG and Er:YAG cases, respectively. The approximation given by Eq. (1) is illustrated in Fig. 3a with the solid red line. With Eq. (1), we estimate $R_{\max} = 1.53 \pm 0.08$ mm for the Nd:YAG case. The average velocity $\dot{R}$ can be estimated as

$$\dot{R} = 2\frac{R_{\max}}{\tau_l} \tag{2}$$

Using $\dot{R}$ and $R_{\max}$, we estimate the inertia timescale τ_{in}

$$\tau_{in} = \frac{R_{\max}}{\dot{R}}. \tag{3}$$

Combining (2) and (3) leads to $\tau_{in} = 0.5\tau_l$. For Nd:YAG case, the pulse duration is much shorter than the inertia timescale, so that the laser energy is assumed to be transformed (deposited) into the bubble energy instantly.

In Er:YAG case, the pulse duration $\tau = 250$ μs is comparable with the bubble lifetime. The maximal radius

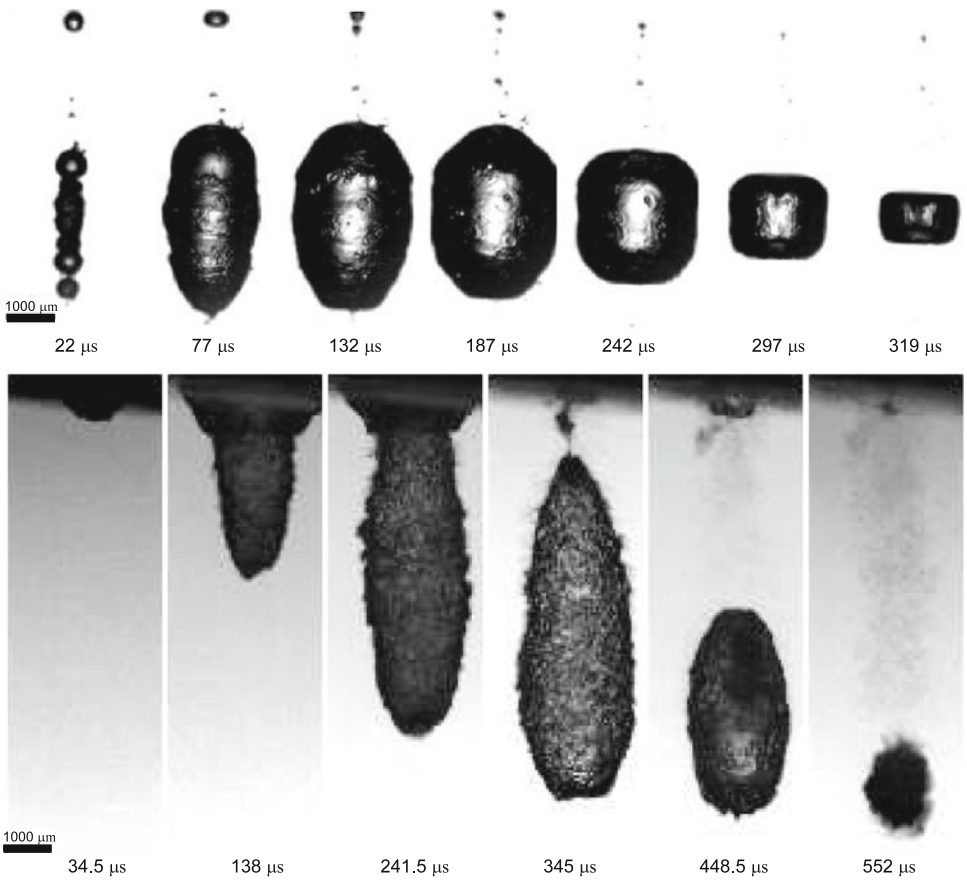

Fig. 2 Sequential images of bubble expansion for Nd:YAG (*top panels*) and Er:YAG (*bottom panels*) cases

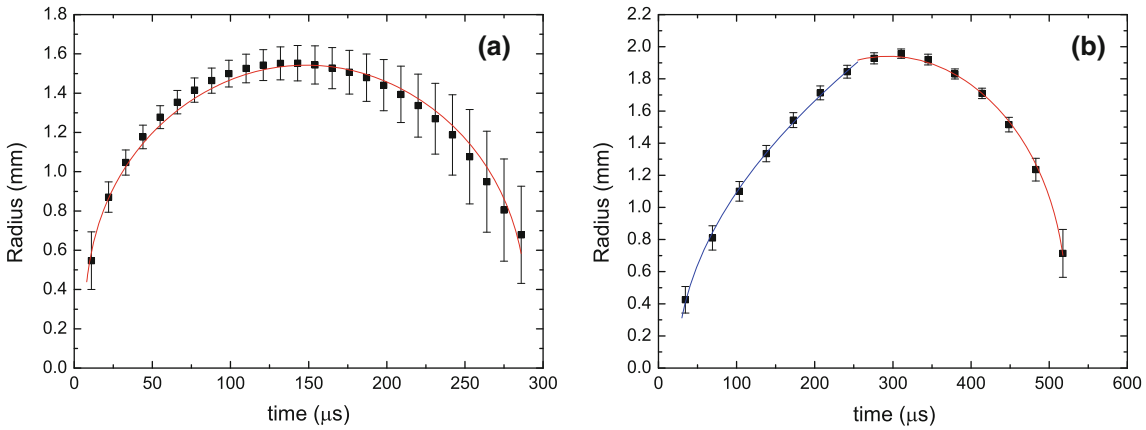

Fig. 3 Measured bubble radius as function of time for Nd:YAG (**a**) and Er:YAG (**b**) cases with analytical approximation given by the *solid line*

is reached when the laser pulse is over, so that during half of the life time we observe the formation of the bubble nuclei. The detailed description of this stage requires explicit description of the processes such as absorption, ionization, and recombination. However, we found that the temporal evolution of the radius during a pulse duration can be approximated by the following power-law dependence

$$R = C_R(t - t_0)^{1/2} \tag{4}$$

where $C_R = 0.1253 \pm 0.0009$ and $t_0 = 23.8 \pm 1$ μs is the time shift between the first captured image and the start of the laser pulse. This dependence is illustrated in Fig. 3b with the solid blue line. The power in Eq. (4) is the same as in the Plesset and Prosperetti [12] equation which describes the temporal evolution of the vapor bubble:

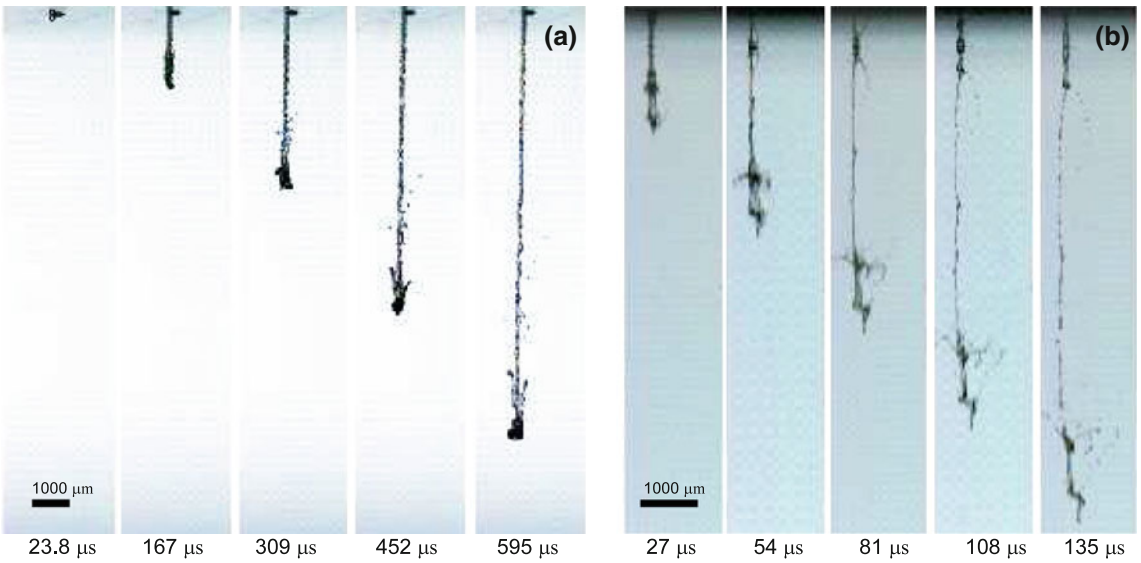

Fig. 4 Sequential images of microjet for Er:YAG (**a**) and Nd:YAG (**b**) cases

$$R = \left(\frac{12}{\pi}\right)^{1/2} \frac{k_1}{L\rho_v} \frac{T_\infty - T_b}{D_l^{1/2}} t^{1/2} \tag{5}$$

where T_b is the boiling temperature, $\rho_v = \rho_v(T_b)$ is the equilibrium vapor density at the boiling temperature, L is the latent heat, and D_l and k_1 are the liquid thermal diffusivity and conductivity, respectively. Adopting typical values of L, D_l, and k_1 we estimate $T_\infty = 156$ °C. Therefore, the expansion of the bubble is similar to a vapor bubble which expands in superheated liquid. While initial stage is strongly affected by the thermal effects in Er:YAG case, the collapse of the bubble and its subsequent rebound is typical for cavitation bubble in both cases.

4 Microjet generation

The mechanism of the jet formation in the microjet device can be described as follows. The laser is focused at the driving liquid (water) inside of a chamber, the laser induces formation of the bubble, the bubble expansion increases the pressure inside of the chamber, the increment of the pressure leads to the deflection of the elastic membrane, and the membrane pushes the drug in the reservoir out through the nozzle. The discharging liquid forms a jet shown in Fig. 1. Figure 4a, b are the sequential images of microjet development for Er:YAG and Nd:YAG cases, respectively.

The velocity of the jet and breakup length are important parameters which determine the skin penetration ability when dealing with trans-dermal drug delivery. The average velocity of the jet driven by Nd:YAG laser is 74 ± 8 m/s while for Er:YAG case, the velocity is 28 ± 4 m/s. Since the main driving mechanism of the jet generation is bubble expansion, the difference in estimated jet velocity can be explained in terms of the average velocity of the bubble. The average velocity is twice higher when the bubble is triggered with Nd:YAG laser than that with Er:YAG one, while the life time is comparable. This leads to a higher pressure gradient in Nd:YAG case, and, consequently, to a higher jet velocity.

The microjet which is generated by Nd:YAG laser breakups into small drops earlier comparing to that for Er:YAG case. The ratio of breakup length to nozzle diameter is 36.9 ± 8.9 and 67.1 ± 0.4 for Nd:YAG and Er:YAG, respectively. The nozzle diameter is 150 μm. Such behavior of liquid jets imply that they belong to a common jet regime where the breakup length decreases with the jet velocity. In this regime, the aerodynamic force is the main factor which induces atomization process. Aerodynamic effects acting on the microjet can be seen from the jet head shape which is illustrated in Fig. 4a, b.

5 Conclusion

We investigate the impact of wavelength and pulse duration on the bubble dynamics and the performance of the laser-induced microjet injector for drug delivery. For Nd:YAG laser, the pulse duration is very short (nanoseconds) relative to the bubble lifetime making the behavior of the bubble close to that of cavitation bubble, while in Er:YAG case, the high absorption in the water and long pulse duration in few microseconds change the initial

behavior of the bubble making it resembling a vapor bubble. The contraction and subsequent rebound are typical for cavitation bubbles in both cases.

The results show that the laser-induced microjet injector generates velocity which is sufficient for the drug delivery. We estimate the typical velocity within 30–80 m/s range and the breakup length to be larger than 1 mm. The range of the breakup length defines the maximal standoff distance if a biomedical injector is to be applied properly. The present study makes important contribution to understanding of the jet-driving mechanism of the laser-induced microjet devices which has been tested successful for transdermal drug delivery in animal tests [5].

Acknowledgments We thank the National Research Foundation of Korea (DOYAK-2010) for financial support through IAAT at Seoul National University. H. Jang and M. Park are also supported by the Korea Ministry of Land, Transport and Maritime Affairs (Haneul Project).

References

1. M.A.F. Kendall, *Handbook of Experimental Pharmacology*, vol. 197, (2010), pp. 193–219
2. M.R. Prausnitz, R. Langer, Nat. Biotechnol. (2008). doi: 10.1038/nbt.1504
3. S. Mitragotri, Nat. Rev. **5**, 543–548 (2006)
4. D.A. Fletcher, D.V. Palanker, Appl. Phys. Lett. **78**, 1933–1935 (2001)
5. M. Park, H. Jang, F.V. Sirotkin, J.J. Yoh, Opt. Lett. **37**, 3894–3896 (2012)
6. T. Han, J.J. Yoh, J. Appl. Phys. **107**, 103110 (2010)
7. I. Akhatov, O. Lindau, A. Topolnikov, R. Mettin, N. Vakhitova, W. Lauterborn, Phys. Fluids **10**, 2805–2819 (2001)
8. A. Vogel, S. Busch, J. Acoust. Soc. Am. **100**, 148–165 (1996)
9. J. Noack, D.X. Hammer, G.D. Noojin, B.A. Rockwell, A. Vogel, J. Appl. Phys. **83**, 7488 (1998)
10. G.M. Hale, M.R. Querry, Appl. Opt. **12**, 555–563 (1973)
11. P.A. Barnes, Studies of laser induced breakdown phenomena in liquid water, Ph.D. Dissertation, 1969
12. M.S. Plesset, A. Prosperetti, Ann. Rev. Fluid Mech. **9**, 145–185 (1977)